University of South Carolina
Scholar Commons

10-7-2011

Synthesis, Structural, Optical and Mechanical Characterization of SrB$_2$O$_4$ Nanorods

Rui Li

Lihong Bao

Xiaodong Li
University of South Carolina - Columbia, lixiao@cec.sc.edu

CrystEngComm

PAPER

Synthesis, structural, optical and mechanical characterization of SrB_2O_4 nanorods

Rui Li, Lihong Bao and Xiaodong Li*

Single crystalline strontium borate (SrB_2O_4) nanorods were synthesized for the first time *via* a facile sol–gel route at low temperature. The SrB_2O_4 nanorods have a good crystalline nature with the growth direction along the [511] orientation and they are transparent from the ultraviolet to the visible regimes. Nanoscale three-point bending tests were performed directly on individual nanorods to probe their mechanical properties using an atomic force microscope. The elastic modulus of SrB_2O_4 nanorods was measured to be 158.2 ± 2.8 GPa, exhibiting a significant increase compared with other borate nanostructures and bulk borates.

Introduction

One dimensional (1D) metal borate nanostructures have attracted tremendous attention due to their outstanding chemical inertness, high temperature stability, excellent mechanical properties, and low thermal expansion coefficient.[1–8] As an important type of optical materials,[9] strontium borates have shown various promising applications in high pressure sensors,[10] magnetooptical media,[11] ultraviolet (UV) phosphors,[12] and detectors for thermoluminescent dosimetry.[13] Guided by the SrO–B_2O_3 phase diagram,[14] five strontium borate bulk materials have been synthesized, which are $Sr_3B_2O_6$, $Sr_2B_2O_5$, SrB_2O_4, SrB_4O_7, and $Sr_2B_{16}O_{26}$.[15] The representative synthesis techniques include solid state reactions between strontium oxide and boric acid and the hydrothermal method. However, to our knowledge, strontium borate nanostructures are still not reported in the literature and their nanoscale-enabled properties are completely unknown.

In our previous work, 1D nanostructures of magnesium borate,[1] aluminium borate,[2] barium borate,[3] and calcium borate[4] have been successfully synthesized. These borate nanostructures exhibit superior mechanical properties. However, the mechanical properties of strontium borates are rarely reported, even for the bulk materials. On the other hand, the optical properties of strontium borate nanostructures have not been explored or theoretically predicted. In this paper, we report the facile synthesis, structural, optical and mechanical characterization of SrB_2O_4 nanorods. Single crystalline SrB_2O_4 nanorods were synthesized for the first time *via* a facile sol–gel route at a relatively low temperature of 800 °C. The X-ray diffraction (XRD) analysis revealed that the as-synthesized nanorods have an

orthorhombic phase of SrB_2O_4 with lattice constants of $a = 12.01$, $b = 4.34$ and $c = 6.59$ Å, and space group of *Pbcn*. The high-resolution transmission electron microscopy (HRTEM) characterization showed that individual SrB_2O_4 nanorods are single crystals with the growth direction along the [511] orientation. The ultraviolet-visible (UV-vis) absorption spectroscopy study unveiled that the SrB_2O_4 nanorods are transparent from the ultraviolet to the visible regimes. Atomic force microscopy (AFM) three-point bending tests were performed directly on individual nanorods to probe their mechanical properties. The elastic modulus of the SrB_2O_4 nanorods was measured to be 158.2 ± 2.8 GPa. Such structural, optical and mechanical information provides design guidelines for developing SrB_2O_4 nanostructure-based nanodevices and nanocomposites, and lays a constitutive foundation for modeling the nanostructures of strontium borates and other borate nanostructures.

Experimental

All chemicals used in our experiments were purchased and used without any further purification. Strontium chloride dihydrate ($SrCl_2 \cdot 2H_2O$) was purchased from Alfa Aesar. Sodium borohydride ($NaBH_4$) and cetyltrimethylammonium bromide (CTAB) were purchased from Sigma Aldrich.

In a typical experiment, 1 mmol of $SrCl_2 \cdot 2H_2O$ and 1.5 mmol of CTAB, and 6 mmol of $NaBH_4$ and 1 mmol of CTAB were separately dissolved in 12 ml distilled water with constant magnetic stirring at room temperature. Then the $NaBH_4$ solution was added dropwise to the $SrCl_2$ solution in 2 min. The reaction mixture was stirred for half an hour, and then stored in air at room temperature without stirring or shaking, and after 48 h a white gel was formed. The as-prepared precursors were placed in an alumina boat and annealed at 800 °C for 1 h in Ar. The white products were washed with distilled water and absolute ethanol three times, respectively, and dried at room temperature.

Department of Mechanical Engineering, University of South Carolina, 300 Main Street, Columbia, South Carolina, 29208, USA. E-mail: lixiao@cec. sc.edu; Fax: (+1) 803-777-0106; Tel: (+1) 803-777-8011

The chemical process for synthesizing SrB_2O_4 nanorods can be described in the following reaction:

$$SrCl_2 \cdot 2H_2O + 2NaBH_4 + 2H_2O = SrB_2O_4 + 2NaCl + 8H_2\uparrow \quad (1)$$
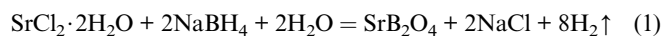
The crystal structure of the products was characterized by XRD (Rigaku DMax 2200 using Cu K_α radiation). A few drops of ethanol solution containing the as-prepared products were deposited onto copper grids for transmission electron microscopy (TEM, Hitachi H-8000), and HRTEM (JEOL JEM 2010F) analyses. The solvent was then vaporized under ambient conditions. The resulting product was collected for characterization by scanning electron microscopy (SEM, Zeiss Ultra Plus FESEM). The UV-vis absorbance spectrum of the as-prepared products was obtained using a Beckman Coulter 640 DU spectrophotometer and quartz cuvettes from Starna. Chemical compositions and oxidation states of the products were determined by X-ray photoelectron spectroscopy (XPS, a Kratos Axis Ultra DLD instrument equipped with a monochromated Al Ka X-ray source and a hemispherical analyzer capable of an energy resolution of 0.5 eV). Thermogravimetric analysis (TGA) and differential thermal analysis (DTA) were carried out using a Thermal Analysis Instruments SDT2960 Thermogravimetric Analyzer with a scan rate of 20 °C per minute. Fourier transform infrared (FTIR) analysis was performed using a Perkin Elmer Spectrum 100 FTIR spectrometer fitted with a Diamond ATR attachment. Nanoscale three-point bending tests were performed directly on individual nanorods to probe their mechanical properties using AFM. To avoid sliding during the bending tests, both ends of the nanorods, which bridged over the trench, were clamped by electron beam induced deposition (EBID) of paraffin in SEM (FEI Quanta 200).[16–18] This carbonaceous material thin layer and the strong adhesion force between the nanorod and the edges of the trench ensured the full clamping of the both ends of the suspended SrB_2O_4 nanorod during the bending tests, and thus the suspended SrB_2O_4 nanorod can be treated as a double clamped beam.

Results and discussion

Fig. 1a shows a representative XRD spectrum of the product synthesized *via* the sol–gel method at 800 °C for 1 h. All the peaks can be readily indexed to the orthorhombic phase of SrB_2O_4 (JCPDS file, No. 84-2175, with lattice constants of $a = 12.01$, $b = 4.34$ and $c = 6.59$ Å, and space group of *Pbcn*). No impurity peaks were observed, indicating high purity of the product. The SEM image of the product shown in Fig. 1b reveals that the product is composed of SrB_2O_4 nanorods with an average diameter of 80 nm and a length ranging from 1 to 3 μm. A high-magnification SEM image shows that the SrB_2O_4 nanorods have a circle-like cross-section (Fig. 1c). The energy dispersive spectroscopy (EDS, Fig. 1d) pattern of the SrB_2O_4 nanorods indicates that the nanorods contain Sr, B and O with the atomic ratio of 18.5 : 29.5 : 52.0, which is comparable to that obtained by XRD. The TEM image (Fig. 1e) shows that the SrB_2O_4 nanorods have very smooth surfaces and the average diameter and length of the nanorod are consistent with the SEM results. The representative HRTEM image (Fig. 1f) and the corresponding
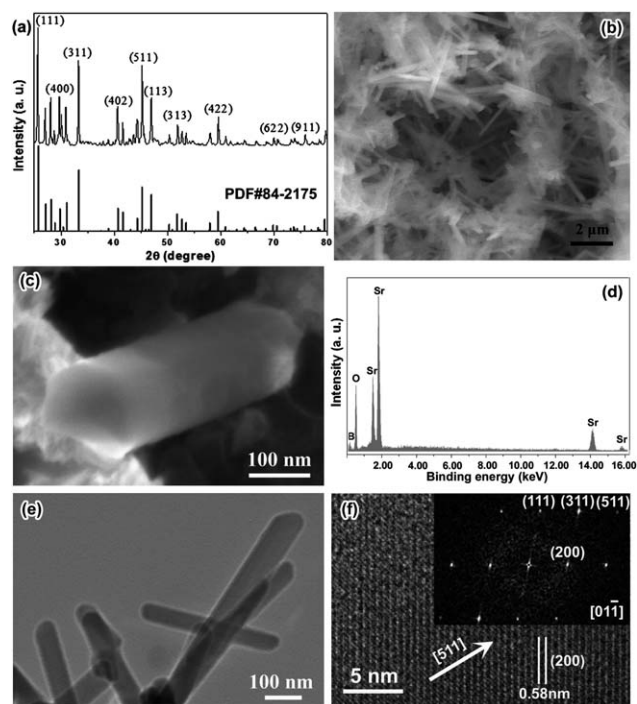

Fig. 1 (a) XRD pattern and the corresponding JCPDS standard pattern (PDF#84-2175), (b and c) SEM images, (d) EDS spectrum, (e) TEM image, (f) HRTEM image and (inset) corresponding FFT pattern of SrB_2O_4 nanorods.

fast-Fourier transform (FFT) pattern at the zone axis of $[01\bar{1}]$ jointly suggest that the synthesized SrB_2O_4 nanorods are single crystals with the growth direction along the [511] orientation, which is consistent with the stronger diffraction intensity of (511) in the XRD pattern in comparison with the standard XRD pattern in Fig. 1a. No defects such as dislocations and twins were found in individual SrB_2O_4 nanorods. The measured distance between the lattice fringes for the (200) planes is 0.58 nm, in good agreement with the XRD results.

To investigate the growth process of the SrB_2O_4 nanorods from the originating precursor (the white color gel obtained from the reaction mixture without heat treatment), both TGA and
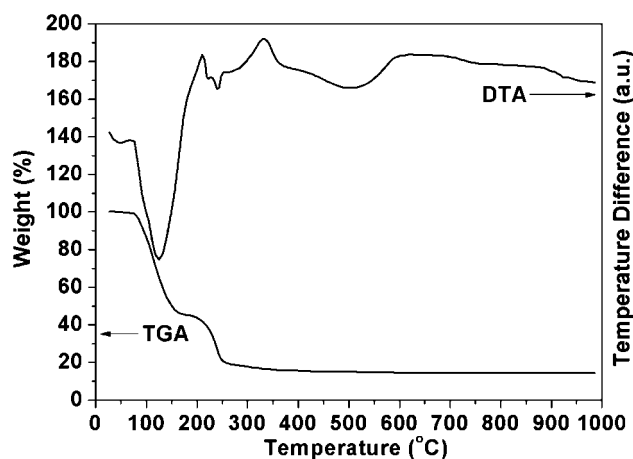

Fig. 2 TGA and DTA curves of the precursor.

DTA were performed, as is shown in Fig. 2. For the precursor, the weight loss was found to be about 82.3% in the range of 25–300 °C when heated in air, in good agreement with the weight loss from the removal of the adsorbed water molecules and the organic groups. Detailed analysis of the TGA curve (Fig. 2) reveals that the weight loss process occurred in two stages, the same as the thermal chemistry process of the reported hydrated borate.[19,20] As determined by EDS, the white color gel (precursor) contains Sr, B, O, C, Na, Cl and Br elements. The contents of C and O reach upto 70 wt%, which indicates that the first stage is related to the removal of the adsorbed water molecules and the hydroxyl groups in the temperature range of 76–180 °C with a weight loss of 55.7%, and the second stage is ascribed to the decomposition of the organic components in the range of 200–300 °C with a weight loss of 26.1%. These two weight loss stages agree well with the two endothermic effects at about 125 °C and 240 °C in the DTA curve (Fig. 2). The exothermic effect at about 600–870 °C can be attributed to the crystallization of the SrB_2O_4 crystals.

XPS analysis was carried out to further characterize chemical compositions of the SrB_2O_4 nanorods (Fig. 3). The binding energies were corrected by taking C 1s at 284.8 eV. The survey spectrum, as shown in Fig. 3a, exhibits Sr 3d, B 1s, O 1s and C 1s core levels, and O Auger peak. In Fig. 3b, the peaks at 133.2 eV and 134.8 eV in the curve can be attributed to Sr $3d_{5/2}$ and Sr $3d_{3/2}$, respectively. In Fig. 3c, the peak at 191.8 eV can be assigned to B 1s core level. In Fig. 3d, the O 1s peak at 531.3 eV suggests that the oxygen exists as O^{2-} species in the SrB_2O_4 nanorods. The XPS results for the SrB_2O_4 nanorods are in good agreement with the reported values for bulk borates.[3,21]

Fig. 4 shows the UV-vis absorption spectrum of SrB_2O_4 nanorods. It can be seen that the SrB_2O_4 nanorods are transparent from 200 nm (5.90 eV) to 1100 nm within the limitation of the instrument, whose working range is 200–1100 nm. The absorption spectrum is relatively featureless, and the broad and overall constant low absorbance from 200 to 1100 nm, including the nearly no absorbance from 200 to 300 nm, is consistent with the reported values for bulk SrB_2O_4 single crystals,[22] demonstrating that the SrB_2O_4 nanorods are transparent from the ultraviolet to the visible regimes. This transparent character indicates that the SrB_2O_4 nanorods are very useful for the optical window application.

Fig. 5 shows the FTIR spectrum of the SrB_2O_4 nanorods. The spectrum exhibits broad absorptions in the 650–1600 cm^{-1} range. Detailed FTIR analysis suggests that the SrB_2O_4 nanorods have all characteristics of bulk SrB_2O_4 crystals. The peak observed at
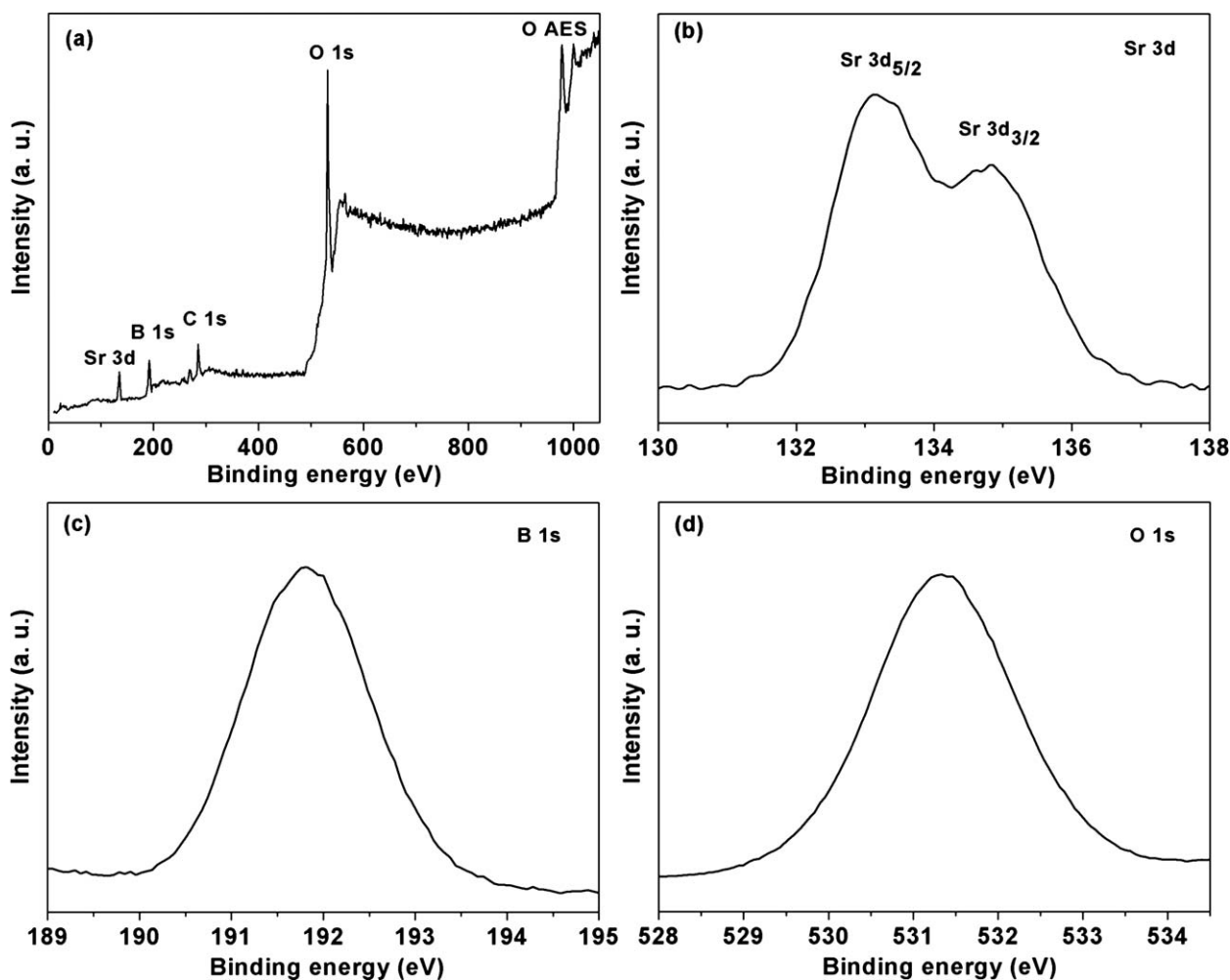

Fig. 3 XPS spectra of SrB_2O_4 nanorods. (a) Survey spectrum, (b)–(d) detailed spectra of Sr 3d, B 1s and O 1s core levels, respectively.
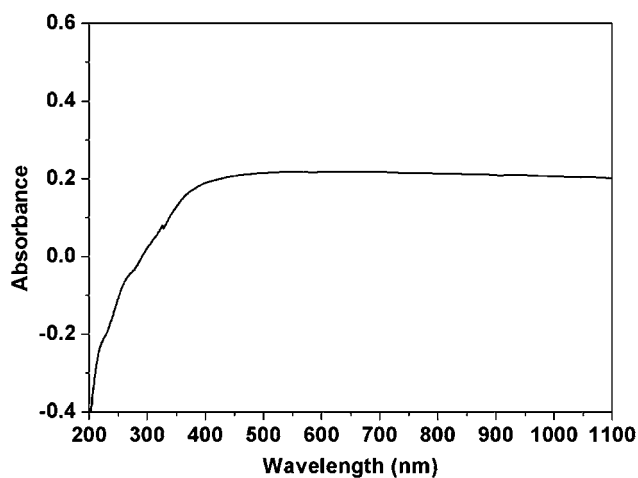
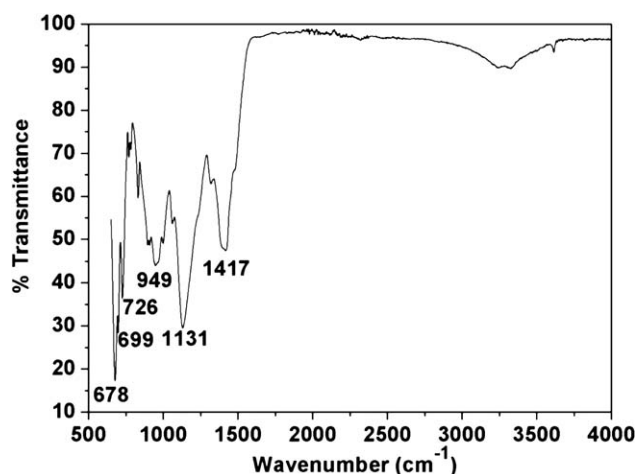**Fig. 4** UV-vis absorption spectrum of SrB_2O_4 nanorods.

Fig. 5 FTIR spectrum of SrB_2O_4 nanorods.

Fig. 6 AFM three-point bending test on an individual SrB_2O_4 nanorod. (a) Schematic image of an EBID-fixed SrB_2O_4 nanorod in a three-point bending test with an AFM tip. (b) SEM and (c) AFM images of a fixed SrB_2O_4 nanorod suspended over the trench. (d) Representative bending force–piezo position (F–Z) curves of the SrB_2O_4 nanorod directly sitting on Si wafer and the SrB_2O_4 nanorod bridging a trench with both ends of the nanorod fixed.

$$E_n = \frac{FL^3}{192 d_n I} = \frac{k_n L^3}{192 I} \tag{2}$$

where I is the moment of inertia. For a circle-shaped nanorod, $I = \pi r^4/4$, where r is the radius of the nanorod. L is the suspended length of the nanorod and F is the applied load at its mid-point position. k_n ($= F/d_n$) is the spring constant of the nanorod, and can be obtained from the equation:[24]

$$k_n = \frac{k_1 k_2}{k_1 - k_2} \tag{3}$$

where k_1 and k_2 are the slopes of the F–Z curves for the SrB_2O_4 nanorod directly sitting on the Si wafer and the suspended SrB_2O_4 nanorod, as shown in Fig. 6d, respectively. The average elastic modulus for the SrB_2O_4 nanorods was measured to be 158.2 ± 2.8 GPa. The mechanical properties of strontium borates have been rarely reported, even for the bulk materials. This is the first time to report the mechanical properties of strontium borates. Our SrB_2O_4 nanorods achieved 25.0%, 25.8%, 30.7%, 53.9%, and 15 720% increase in elastic modulus compared with $Ca_2B_2O_5 \cdot H_2O$ nanobelts,[4] $Mg_2B_2O_5$ nanowires,[1] $Al_{18}B_4O_{33}$ nanowires,[2] $Al_4B_2O_9$ nanowires,[2] and $Ca_2B_2O_5$ nanogrooves,[4] respectively. The observed elastic modulus is also 1.8%, 60.8% increase compared with bulk borates: $Mg_2B_2O_5$,[1] $Ca_2B_2O_5$,[25] respectively; 60.5% decrease compared with bulk $Al_{18}B_4O_{33}$.[26] These findings are significant for designing strontium borate nanostructure-based nanocomposites and nanodevices, and lay a constitutive foundation for modeling the nanostructures of strontium borates and other borate nanostructures.

Conclusions

In summary, single crystalline strontium borate (SrB_2O_4) nanorods were synthesized for the first time *via* a facile sol–gel route at

949 cm^{-1} is attributed to B–O extra-ring stretching.[3] The bands at about 897 cm^{-1} are due to the BO_3 symmetric stretching modes. The band at 1417 cm^{-1} is due to the asymmetric stretching vibration of the group BO_3. The band at 1131 cm^{-1} is assigned to the in-plane bending of the group BO_3. The bands observed at 726, 699, and 678 cm^{-1} are due to the out-of-plane bending mode of the group BO_3. The FTIR spectrum confirms the existence of the trigonally coordinated boron atoms, consistent with the crystallographic study.[23]

Nanoscale three-point bending tests[17,24] were performed directly on individual SrB_2O_4 nanorods to probe their mechanical properties (Fig. 6a). To avoid sliding during the bending tests, both ends of the nanorod, which bridged over the trench, were clamped by EBID of paraffin.[16–18] Fig. 6b and c are representative SEM and AFM images of an EBID-fixed nanorod, respectively. Fig. 6d shows representative force–piezo position (F–Z) curves obtained along the Z-direction on the nanorod directly sitting on a Si wafer and the suspended nanorod, respectively. The F–Z curves exhibit a strong linear relationship up to 450 nN. On the basis of elastic beam-bending theory, the elastic modulus of SrB_2O_4 nanorods, E_n, can be calculated from the equation:[17,24]
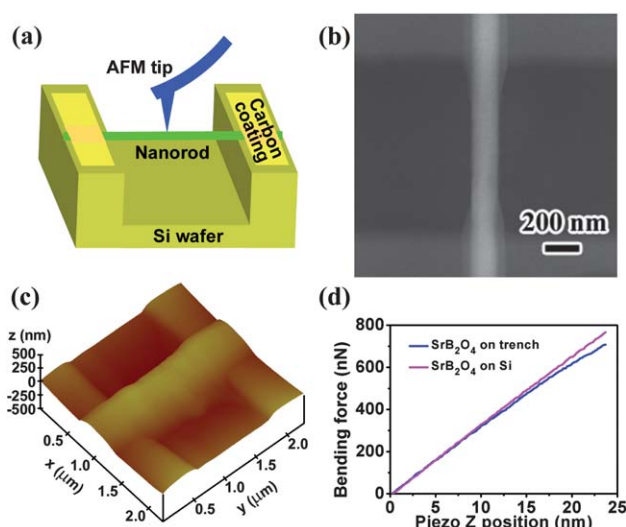
low temperature. The SrB_2O_4 nanorods are transparent from the ultraviolet to the visible regimes. AFM-based nanoscale three-point bending tests were performed on individual SrB_2O_4 nanorods to probe their mechanical properties and the average bending elastic modulus is 158.2 ± 2.8 GPa, exhibiting a significant increase compared with other borate nanostructures and bulk borates.

Acknowledgements

References

1 X. Y. Tao and X. D. Li, *Nano Lett.*, 2008, **8**, 505–510.
2 X. Y. Tao, X. N. Wang and X. D. Li, *Nano Lett.*, 2007, **7**, 3172–3176.
3 R. Li, X. Y. Tao and X. D. Li, *J. Mater. Chem.*, 2009, **19**, 983–987.
4 L. H. Bao, Z. H. Xu, R. Li and X. D. Li, *Nano Lett.*, 2010, **10**, 255–262.
5 Y. Li, Z. Y. Fan, J. G. Lu and R. P. H. Chang, *Chem. Mater.*, 2004, **16**, 2512–2514.
6 R. Z. Ma, Y. Bando, T. Sato, C. C. Tang and F. F. Xu, *J. Am. Chem. Soc.*, 2002, **124**, 10668–10669.
7 C. C. Tang, E. M. Elssfah, J. Zhang and D. F. Chen, *Nanotechnology*, 2006, **17**, 2362–2367.
8 Y. C. Zhu, Y. Bando and R. Z. Ma, *Adv. Mater.*, 2003, **15**, 1377–1379.
9 T. I. Korshikova, S. V. Parkhomenko, A. V. Tolmachev, V. A. Tsurikov and R. P. Yavetskiy, *Inorg. Mater.*, 2008, **44**, 1345–1348.
10 F. Datchi, R. LeToullec and P. Loubeyre, *J. Appl. Phys.*, 1997, **81**, 3333–3339.
11 A. S. Aleksandrovsky, A. V. Malakhovskii, V. N. Zabluda, A. I. Zaitsev and A. V. Zamkov, *J. Phys. Chem. Solids*, 2006, **67**, 1908–1912.
12 D. S. Thakare, S. K. Omanwar, P. L. Muthal, S. M. Dhopte, V. K. Kondawar and S. V. Moharil, *Phys. Status Solidi A*, 2004, **201**, 574–581.
13 M. Santiago, A. Lavat, E. Caselli, M. Lester, L. J. Perisinotti, A. K. de Figuereido, F. Spano and F. Ortega, *Phys. Status Solidi A*, 1998, **167**, 233–236.
14 C. F. Chenot, *J. Am. Ceram. Soc.*, 1967, **50**, 117–118.
15 Z. H. Tang, X. A. Chen and M. Li, *Solid State Sci.*, 2008, **10**, 894–900.
16 W. Ding, D. A. Dikin, X. Chen, R. D. Piner, R. S. Ruoff, E. Zussman, X. Wang and X. Li, *J. Appl. Phys.*, 2005, **98**, 014905.
17 H. Ni, X. D. Li and H. S. Gao, *Appl. Phys. Lett.*, 2006, **88**, 043108.
18 H. Ni, X. D. Li, G. S. Cheng and R. Klie, *J. Mater. Res.*, 2006, **21**, 2882–2887.
19 Z. H. Liu and H. S. Huang, *Thermochim. Acta*, 2006, **448**, 59–62.
20 H. S. Huang and Z. H. Liu, *Thermochim. Acta*, 2007, **463**, 87–89.
21 G. D. Khattak, N. Tabet and M. A. Salim, *J. Electron Spectrosc. Relat. Phenom.*, 2003, **133**, 103–111.
22 J. B. Kim, K. S. Lee and J. N. Kim, *Mater. Lett.*, 1997, **31**, 93–97.
23 J. B. Kim, K. S. Lee, I. H. Suh, J. H. Lee, J. R. Park and Y. H. Shin, *Acta Crystallogr., Sect. C: Cryst. Struct. Commun.*, 1996, **52**, 498–500.
24 X. Y. Tao, L. X. Dong, X. N. Wang, W. K. Zhang, B. J. Nelson and X. D. Li, *Adv. Mater.*, 2010, **22**, 2055–2059.
25 Manupriya, K. S. Thind, G. Sharma, V. Rajendran, K. Singh, A. V. G. Devi and S. Aravindan, *Phys. Status Solidi A*, 2006, **203**, 2356–2364.
26 S. C. Tjong and W. Jiang, *J. Appl. Polym. Sci.*, 1999, **73**, 2247–2253.